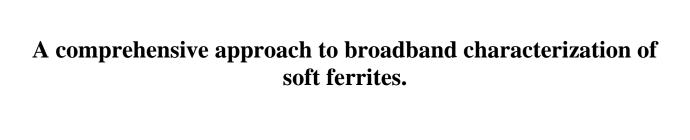


# ISTITUTO NAZIONALE DI RICERCA METROLOGICA Repository Istituzionale

A comprehensive approach to broadband characterization of soft ferrites

This is the author's submitted version of the contribution published as:
Original A comprehensive approach to broadband characterization of soft ferrites / Beatrice, Cinzia; Fiorillo, F In: INTERNATIONAL JOURNAL OF APPLIED ELECTROMAGNETICS AND MECHANICS ISSN 1383-5416 48:2-3(2015), pp. 283-294. [10.3233/JAE-152000]
Availability: This version is available at: 11696/32624 since: 2021-01-28T14:59:08Z
Publisher: IOS Press
Published DOI:10.3233/JAE-152000
Terms of use:
This article is made available under terms and conditions as specified in the corresponding bibliographic description in the repository
Publisher copyright

(Article begins on next page)



F. Fiorillo and C. Beatrice

<sup>1</sup>Istituto Nazionale di Ricerca Metrologica (INRIM), Strada delle cacce 91, 10135 Torino, Italy

### 1 Abstract

We present and discuss methods, setups, and results concerning the characterization of Mn-Zn and Ni-Zn ferrites in the frequency range DC - 1 GHz, by which we bring to light the physical mechanisms responsible for the observed frequency behavior of magnetic losses W and permeability  $\mu$  and provide thorough assessment of the broadband response of the material. A comprehensive array of polarization  $J_p$  and frequency f values is investigated. A fluxmetric approach is applied up to a few MHz, giving way to a transmission line method at higher frequencies, up to 1 GHz. The fluxmetric measurements are made at defined  $J_p$  value, typically from a few mT to some hundred mT. The waveguide characterization, centered on the use of a network analyzer, is instead made under defined exciting power. But a full experimental  $W(J_p, f)$  matrix up to 1 GHz and  $J_p$  values typically belonging to the Rayleigh region is in any case retrieved, thanks to the linear response of the material at high-frequencies. Disaccommodation measurements are the route followed in these experiments to separate the rotations from the domain wall process at all frequencies. Whatever the magnetization mode, the role of eddy currents in Mn-Zn ferrite losses is put in evidence by means of resistivity measurements and ensuing multiscale numerical modeling, the loss experiments being made on progressively thinned ring samples. It is concluded that an eddy current free  $W(J_p, f)$  behavior can always be obtained, which can be decomposed into domain wall and rotation related contributions. The latter can be calculated assuming a suitable distribution of the effective internal anisotropy fields and its introduction in the Landau-Lifshitz-Gilbert derivation of the rotational susceptibility.

2728

29

2

3

4

5

6

7

8

9

10

11

12

13

14

15

16

17

18

3031

#### 1. Introduction

32

33

34

35

36

37

38

39

40

41

42

43

44

45

46

47

48

49

50

51

52

53

54

55

Mn-Zn and Ni-Zn sintered ferrites are the materials of choice for applications where high permeability and low losses are required in a vast range of frequencies [1, 2]. But the physical interpretation of the ferrite behaviour, namely magnetic loss and permeability, across the broad frequency domain useful for the various applications in electrical, electronic, and telecommunication devices, lags behind today's technological developments. This derives in part from lack of comprehensive magnetic characterization, typically restricted in the literature to relatively narrow ranges of frequency and polarization values [3-5]. These materials do actually display a complex magnetic phenomenology, where domain wall (dw) processes and magnetization rotations, combining in comparable proportions under DC excitation, evolve with the magnetizing frequency through different dissipation channels, descending from eddy current and spin damping phenomena. Experiments should then possibly aim at identifying and separating the different types of magnetization processes and the underlying dissipation mechanisms. In this paper we discuss an ensemble of methods and experiments we have developed for the characterization of the magnetic properties of Mn-Zn and Ni-Zn ferrites from quasi static excitation to microwave frequencies, that is, up to full relaxation of the material response. We show how fluxmetric and transmission line measuring methods seamlessly combine to provide a broad matrix of values of the complex permeability and the energy loss as a function of peak polarization  $J_p$  and frequency f. The role of eddy currents in Mn-Zn ferrites is brought to light measuring the electrical resistivity versus f and making loss measurements as a function of the sample thickness. The electrical and magnetic results are reconciled by multiscale modelling of eddy current circulation in the real heterogeneous material. The ubiquitous presence of the magnetic aftereffect is exploited to separate the dw and rotational contributions to the magnetization process. By disaccommodation experiments performed versus frequency it is verified, in particular, that the dw processes subside, in general, on entering the MHz range, and magnetization rotations prevail. These display damped resonant response, with local resonance frequencies distributed according to the distribution of the local effective anisotropy fields, the combination of magnetocrystalline anisotropy and internal demagnetizing fields.

5657

58

59

60

61

62

63

64

65

66

67

## 2. Measurement of the electrical resistivity.

Knowledge of the electrical resistivity and its dependence on frequency is basic to the analysis of the energy losses of the Mn-Zn sintered ferrites. The typically measured resistivity values are in fact compatible, contrary to the case of the nearly insulating Ni-Zn ferrites, with the existence of eddy current generated losses [1, 5, 6, 7]. Efforts are therefore spent towards loss reduction by increasing the resistivity through addition of segregating oxides, like CaO, SiO<sub>2</sub>, Nb<sub>2</sub>O<sub>5</sub>, TiO<sub>2</sub>, and fine control of the partial pressure of oxygen during sintering [4, 8, 9]. It can be shown, however, that the eddy current loss contribution can be suppressed, at least below a few MHz, if the sample is sufficiently mall [10]. This finding can be quantitatively assessed by modelling the eddy current behaviour versus frequency, where the real heterogeneous structure of the sintered material, where the semiconducting grains are separated by nearly insulating boundary layers, is taken into

account [11]. The capacitive properties of the nanometer-thick grain boundaries, resulting into an extremely high value of the relative permittivity of the sintered material (a few 10<sup>4</sup>), leads to eddy currents evolving with increasing frequency from local, grain boundary limited, to intergrain patterns, eventually investing the whole sample cross-section [9].

The real  $\rho$ ' and imaginary  $\rho$ '' resistivity components of the investigated Mn-Zn ferrites have been determined by means of standard four-wire measurements of the electrical impedance of cut rings, where good voltmetric and amperometric electrical contacts are ensured at the sample ends by sandwiching indium strips between the freshly polished sample surface and the copper leads and applying uniform pressure. The temperature of the sample, which was kept in a temperature controlled plastic chamber, was controlled up to T = 140 °C by means of microthermocouple stuck on it. The impedance was measured up to f = 15 MHz either by an Agilent 4294A LCR meter or a built-on-purpose setup employing an Agilent 33220A function generator and a 500 MHz Tektronix TDS814 oscilloscope.

The simplest way to describe the electrical behavior of the Mn-Zn sintered ferrites consists in adopting the equivalent RC circuit shown in Fig. 1a, where the response of the grains and their boundary layers is described through the resistance  $R_g$  (the grains) and the parallel of a capacitance  $C_b$  and a resistance  $R_b$  (the boundary). More complex equivalent circuits can actually be envisaged, by additionally considering the capacitance of the grains and possible self-inductance effects [5] and by distinguishing between intrinsic and extrinsic grain boundaries and the related resistance-capacitance equivalent circuits [9]. It appears, however, that the circuit in Fig. 1a of impedance

$$Z(f) = R_{\rm g} + R_{\rm b} / (1 + \omega^2 R_{\rm b}^2 C_{\rm b}^2) - j\omega R_{\rm b}^2 C_{\rm b} / (1 + \omega^2 R_{\rm b}^2 C_{\rm b}^2)$$
 (1)

can satisfactorily emulate the electrical response of all the investigated Mn-Zn ferrites, as shown by the example provided in Fig. 1, where the correspondingly predicted behaviors of  $\rho'(f)$  and  $\rho''(f)$  for an N87-type ferrite at room temperature and at T=100 °C (dashed lines) are compared with the experiments. By assimilating the sample as an ordered assembly of cubic grains of side equal to the measured average grain size  $\langle s \rangle$ , we can estimate, according to the predicted resistivities  $\rho'(f)$  and  $\rho''(f)$ , the resistivity of the grain  $\rho_g$  and the parameters of the boundary layer: resistivity  $\rho_b$ , thickness  $\delta$ , and permittivity  $\epsilon = \epsilon_0 \epsilon_r$ . These quantities are shown for the N87-type ferrite, where  $\langle s \rangle = 16$   $\mu$ m, in Table I. The estimated  $\delta$  value, of the order of the elementary cell size, appears somewhat lower than the actual grain boundary thickness, as revealed by electron transmission microscopy [4, 5]. One might actually consider  $\delta$  as an electrically equivalent thickness, which is expected to attain the nanometer value in ferrites with high relative permittivity (say around  $10^5$ ) [12]. It is observed in Table I that, according to the observed behaviour of  $\rho'(f)$  and  $\rho''(f)$  and Eq. (1), the increase of temperature affects to considerable extent only the resistivity of the boundary layer.

## 2. Domain wall displacements versus rotational processes.

Soft ferrites are characterized by very low magnetocrystalline anisotropy, resulting from the mechanism of anisotropy compensation [13], and high permeability values can be obtained upon the temperature range useful for applications. Magnetization rotations and dw displacements require then comparable driving fieldstrengths and combine all along the magnetization curve. It is widely held, that, contrary to the case of conventional Febased polycrystalline soft magnets [14], the rotational processes may play a dominant role at low inductions [15, 16], where most broadband applications lie, but it is difficult to quantify their contribution and the related frequency dependence. At such inductions one may indeed take advantage of the pseudoellipsoidal shape of the DC hysteresis loop and provide meaning to its evolution with frequency through the behaviour of the real  $\mu$ ' and imaginary  $\mu$ '' permeability components. The energy loss) can in such a case be expressed as

$$W(J_{p}) = \pi J_{p}^{2} \mu'' / (\mu'^{2} + \mu'^{2}) [J/m^{3}].$$
(2)

Nakamura, et al. [17, 18] proposed to separate dw  $\mu_{dw}$  and rotational  $\mu_{rot}$  initial permeabilities and their frequency dependence in Ni-Zn sintered ferrites by postulating resonant and relaxation response for  $\mu_{dw}$  and  $\mu_{rot}$ , respectively, and making best fitting of the measured  $\mu$ ' and  $\mu$ '' by means of five adjustable parameters. The so obtained  $\mu$ 'dw(f),  $\mu$ ''rot(f), and  $\mu$ ''rot(f) behaviours are, however, highly hypothetical and basically unproved. In this work we have separately identified the complex permeabilities  $\mu_{dw}(f)$  and  $\mu_{rot}(f)$  combining the measurement of the initial magnetization curve with experiments on the time decay of the initial permeability (disaccommodation). Examples of quasi-static initial magnetization curves, limited to their low-field portion ( $J_p \le 50 - 100$  mT) are provided in Fig. 2a. It is the induction region of actual interest for most broadband applications of soft ferrites, where, as shown in Fig. 2a, the constitutive equation J(H) closely follows the Rayleigh law  $J = aH + bH^2$  and the permeability is a linear function of the field  $\mu(H) = a + bH$  (Fig. 2b). A reversible term aH, where  $a = \lim_{H\to 0} \mu(H)$  is the initial permeability, and an irreversible contribution  $bH^2$  are thus identified. The irreversible magnetization is exclusively provided by the dw displacements, while both rotations and dw motion combine to provide the reversible term. Assuming a uniform distribution of the easy axes of the polycrystalline material, it is obtained that the rotational permeability is to good approximation constant in a large part of the Rayleigh region.

Permeability and energy losses have been measured in Mn-Zn and Ni-Zn ring samples at different  $J_p$  values, starting from  $J_p = 1$  mT, from a few hundred Hz (quasi-static regime) up to about 10 MHz by means of a calibrated hysteresisgraph/wattmeter. These measurements remarkably show that within the previous restricted  $J_p$  limits the  $\mu'(f)$  and  $\mu''(f)$  curves (and, *a fortiori*, the W(f) curves) all collapse onto a single curve [19], as illustrated for two  $J_p$  values in the example given in Fig. 3. This permits us to extend the experimental frequency band towards the GHz range by relaxing the requirement of a defined measuring value of  $J_p$ . We have applied for this a transmission line method, using a Vector Network Analyzer (Agilent 8753A), where the complex permeability is obtained between about 1 MHz and 1 GHz by measuring the impedance of the ferrite ring sample, placed at the bottom of a shorted coaxial line, in reflection mode under constant incident power P

= 10 mW [20]. Fig. 3 provides some important piece of information. Based on our previous analysis of the Rayleigh diagram, we can state first that any difference  $\mu'_{\text{diff}} = \mu'(J_{p2}) - \mu'(J_{p1})$ , with  $J_{p2} > J_{p1}$ , is entirely associated with the dw processes and can be written as  $\mu'_{\text{diff}} = \mu'_{\text{dw}}(J_{\text{p2}}) - \mu'_{\text{dw}}(J_{\text{p1}})$ . From the observed frequency dependence of  $\mu'_{diff}(f)$  it is recognized that the dw dynamics is of relaxation type. The hump on the  $\mu'(f)$  curve, the landmark trait of ferromagnetic resonance, thus originates in the rotational process. It tends to drown into the increasing contribution by the relaxation-type dw term  $\mu'_{dw}$  with increasing  $J_p$ . Coalescing of the different  $\mu'(J_p)$  curves at high frequencies is thus simply understood as a consequence of the decrease and disappearance of  $\mu'_{dw}(f)$  beyond the relaxation frequency, the surviving rotational term  $\mu'_{rot}(f)$  being, as previously remarked, quite independent of  $J_p$  in the Rayleigh region. The relaxation character of the dw dynamics is confirmed by disaccommodation experiments, where the decay of the initial permeability versus time under a weak AC field is measured immediately after the demagnetization process. Disaccommodation is exclusively related to the dws, whose oscillatory motion slightly shrinks with time under the stabilizing action of diffusing cations. We have shown in a previous work [11] that the rate of decay of  $\mu$ ' (of logarithmic type) in Mn-Zn ferrites decreases with increasing the frequency of the exciting field in a way totally consistent with a relaxation dispersion of the dw permeability, eventually tending to revert, according to the theory, to a slight increase beyond the cutoff frequency. This equally happens in Ni-Zn ferrites, as demonstrated in Fig. 4 by the time dependence of the reduced permeability  $\mu'(t)/\mu'(t_0)$ , with  $t_0 = 2$  s, measured at field frequencies ranging between 500 kHz and 2 MHz.

Having clarified the nature of the dispersion of  $\mu_{r,dw}(J_p)$ , we can turn to quantitative discrimination between the dw and rotational permeabilities, again exploiting disaccommodation. The idea is one of comparing the permeability decays starting from the demagnetized state and from remanence (major loop). The former condition is attained by conventional demagnetization procedure at 50 Hz, the latter by sudden release of a saturating DC field. The strength of the weak AC exciting field is such as to engender a quasi-reversible polarization swing, typically  $\Delta J = \pm 2$  mT. In the limit of small oscillations the rotational susceptibility can be written, for easy axes of anisotropy constant K distributed according to an angular function  $g(\theta)$ ,

$$\chi_{\text{rot}} = \int_{-\pi/2}^{\pi/2} (\mu_0 M_s^2 / 2K) \cdot \sin^2 \theta \ g(\theta) d\theta \,, \tag{3}$$

where  $M_s$  is the saturation magnetization. Since  $\sin^2\theta = \sin^2(\pi - \theta)$ , all quadrants are equivalent and  $\chi_{rot}$  is the same for small moment rotations occurring either at remanence  $(J = J_r)$  or in the demagnetized state (J = 0). The difference  $\Delta\mu$  between the small amplitude permeabilities observed in these two states is therefore entirely ascribed to the lower domain wall contribution at remanence  $\Delta\mu(t) = \mu_{dw}(J = 0, t) - \mu_{dw}(J = J_r, t)$ . Fig. 5 shows that the permeability, taken at f = 10 kHz, decays slightly faster in the demagnetized state. Since the derivative  $D = d\mu/d(\log t)$  can be taken approximately proportional to  $\mu_{dw}$  at any time t [21], we can also write

$$\mu_{\text{dw}}(J=0,t)/\mu_{\text{dw}}(J=J_{\text{r}},t) = D(J=0,t)/D(J=J_{\text{r}},t),$$
 (4)

where the time t of interest is the one where the loss measurement is performed after demagnetization, typically around  $10^3$  s. Combining at this time the previous equations and further taking into account that with f = 10 kHz  $\mu(t) \cong \mu'(t)$  and  $\mu'(t) \cong \mu'_{DC}$ , we obtain the dw contribution to the real permeability component under quasi-static excitation

176 
$$\mu'_{\text{dw, DC}}(J=0) = \frac{\Delta\mu}{1 - D(J=J_{r})/D(J=0)},$$
 (5)

at the low  $J_p$  level impressed by the AC field ( $J_p = 2$  mT for the case of Fig. 5). We estimate for such a case the relative permeabilities  $\mu'_{r,dw,DC} = 445$  versus  $\mu'_{r,DC} = 2040$  (N87 ferrite) and  $\mu'_{r,dw,DC} = 695$  versus  $\mu'_{r,DC} = 4540$ (N30 ferrite). Having thus estimated  $\mu'_{dw,DC}$  ( $J_p = 2$  mT), it is an easy matter to retrieve the whole  $\mu'_{dw}(f)$ behaviours at the different  $J_p$  values exploiting the previously introduced experimental quantities  $\mu'_{\text{diff}}(f, J_{\text{pi}}) =$  $\mu'(f, J_{pi}) - \mu'(f, J_{p} = 2 \text{ mT}) = \mu'_{dw}(f, J_{pi}) - \mu'_{dw}(f, J_{p} = 2 \text{ mT})$ . We can in fact estimate  $\mu'_{dw}(f, J_{p} = 2 \text{ mT})$ assuming it replicates the frequency dependence of the experimental  $\mu'_{diff}(f, J_{pi} = 5 \text{ mT})$ , while tending to the calculated  $\mu'_{dw,DC}$  ( $J_p = 2$  mT) at low frequencies. It is then immediate to calculate  $\mu'_{dw}(f, J_{pi})$  at all  $J_{pi}$  values, till an upper limit roughly identified by the Rayleigh law. Quite a similar procedure, passing through the etermination of the experimental quantity  $\mu''_{\text{diff}}(f, J_{\text{pi}}) = \mu''(f, J_{\text{pi}}) - \mu''(f, J_{\text{p}} = 2 \text{ mT}) = \mu''_{\text{dw}}(f, J_{\text{pi}}) - \mu''_{\text{dw}}(f, J_{\text{pi}})$ 2 mT), can be applied in order to retrieve the imaginary component  $\mu''_{dw}(f, J_{pi})$ . Now the low-frequency limit is given by the condition  $\mu''_{dw,DC}$   $(J_p = 2 \text{ mT}) \equiv \mu''(J_p = 2 \text{ mT})$ , because the quasi-static energy loss is exclusively generated by the dw processes. Fig. 6 compares the so-extracted  $\mu'_{dw}(f, J_{pi})$  and  $\mu''_{dw}(f, J_{pi})$ behaviours with the measured permeability components  $\mu'(f, J_{pi})$  and  $\mu''(f, J_{pi})$ , in the  $J_p$  range 2 mT – 50 mT (Mn-Zn ferrite N87). The relaxation character of the dw dynamics leads to vanishing of  $\mu'_{r,dw}(f)$  and  $\mu''_{r,dw}(f)$ on entering the MHz range, where they are completely superseded by the rotational terms. These are associated with the resonant response of the material, as illustrated by the peaked behaviour  $\mu'_{r,rot}(f) = \mu'_r(f) - \mu'_{r,dw}(f)$  in Fig. 7.

### 3. Energy losses.

172

173

174

175

177

178

179

180

181

182

183

184

185

186

187

188

189

190

191

192

193

194195

196

197

198

199

200

201

202

203

204205

We have remarked that the phenomenology of energy losses can be viewed in terms of complex magnetic permeability, as synthetically shown by Eq. (1). The previous analysis gives then us the opportunity to discriminate between the loss contributions originating from the dw and the rotational processes.

Writing the expression for the energy loss at a given  $J_p$  value as

$$W(J_{\rm p}) = \pi J_{\rm p}^2 (\mu''_{\rm dw} + \mu''_{\rm rot}) / (\mu'^2 + \mu''^2) = W_{\rm dw} (J_{\rm p}) + W_{\rm rot} (J_{\rm p}), \qquad [\rm J/m^3]$$
 (6)

and taking the  $\mu$ ''<sub>dw</sub> and  $\mu$ ''<sub>rot</sub> dependence on frequency obtained through the previously discussed procedure (see Fig. 7), we arrive at the decomposition of the loss in its dw and rotational components. Fig. 8 provides an example of the so-obtained  $W_{dw}(f)$  and  $W_{rot}(f)$  behaviours at two different  $J_p$  values in a Mn-Zn N87-type ring sample (outside diameter 15 mm, inside diameter 10.4 mm, thickness 5.09 mm). It is noted that  $W_{dw}(f)$  and  $W_{rot}(f)$  comparably contribute to W(f) in a relatively narrow intermediate frequency interval only. It is also

observed that, according to Eq. (6),  $W_{rot}(f)$  strictly follows a  $J_p^2$  law, being  $\mu''_{rot}$  independent of  $J_p$ , while  $W_{dw}(f)$  grows faster, because  $\mu''_{dw}$  increases with  $J_p$  (see Fig. 6). Consequently, overlapping between the fluxmetric and transmission line measurements occurs over a shrinking region on increasing  $J_p$ . In this region, a relatively sharp transition of the slope of the W(f) curve occurs. It might be argued that such a transition could be related in some way to the concurring drop of the electrical resistivity (see Fig.1), thereby implying an important contribution to the losses by the eddy currents. This is not the case. A same W(f) behaviour is in fact observed in the insulating Ni-Zn ferrites [22] and in sufficiently small Mn-Zn samples, like the ones considered in Fig. 8. Eddy current losses in the sintered Mn-Zn ferrites have important practical implications, as demonstrated by the constant efforts devoted to the development of materials with increased grain boundary resistivity [4], but their calculation is difficult, because of the electrically heterogeneous structure of the material. Their role is in any case apparent when measuring the losses in differently sized Mn-Zn samples. The general literature approach to the calculation of eddy current losses is one of applying the conventional formulation for a homogeneous material (classical loss  $W_{class}(J_p, f)$ ), which, for a circular sample of diameter d is simply expressed as

220 
$$W_{\text{class}}(J_{p}, f) = \frac{\pi^{2}}{16\rho'(f)} \cdot d^{2}J_{p}^{2}f, \qquad (7)$$

where  $\rho'(f)$  is the real resistivity component, as obtained with the measurements reported in Fig. 1. It has been shown, however, that Eq. (7) can largely overestimate the actual eddy current losses and can be reconciled with a correct formulation only at very high frequencies in [11]. Because of the insulating character of the grain boundary layer, eddy currents at low frequencies circulate inside the grains and the ensuing energy dissipation is much lower than the one predicted using the measured  $\rho'(f)$  in Eq. (7), which amounts to assume eddy current patterns freely investing the sample cross-section. The general problem of calculating the eddy current losses in the sintered Mn-Zn ferrites has been discussed in [11], where the electromagnetic field equations in the heterogeneous material are formulated under a variational multiscale approach and numerically implemented by means of finite element method, by which the evolution of the eddy current patterns from grain limited to global upon increasing frequency can be described. It is obtained, in particular, that the numerical results can be fitted by the closed expression

$$W_{\text{eddy}}^{\text{(cl)}}(J_{p}, f) = \left\{ \frac{(k_{0} - k_{\infty})A}{1 + \exp[m \log_{10}(f/f_{0})]} + k_{\infty}A \right\} J_{p}^{2} f, \qquad [J/m^{3}]$$
(8)

where  $k_0AJ_p^2$  and  $k_\infty AJ_p^2$  are the calculated limits of  $W_{\rm eddy}^{\rm (cl)}(J_p,f)/f$  for  $f{\to}0$  (eddy currents confined in a single grain, typically below a few kHz) and  $f{\to}\infty$  (eddy currents circulating across the whole sample cross-section, typically beyond a few MHz), respectively. Eq. (8) provides a "classical contribution" (it will actually tend to  $W_{\rm class}(J_p,f)$  at high frequencies), because the calculation does not take into account the role of the moving domain walls and the ensuing local eddy currents. The related contribution (the excess eddy current loss) has

whole of the eddy current losses. The quantity A is an effective area, depending on the width-to-thickness ratio w/h. It is related to the actual cross-sectional area S as A = gS, where g is geometrical constant given by  $g = 1 - 0.0923 (p-1)^{1.63}$  and p = w/h if w > h and p = h/w if h > w. Each material is associated with a defined set of parameters  $k_0$ ,  $k_{\infty}$ , m, and  $f_0$ , where the constants m and  $f_0$  are obtained from best fitting of the curves calculated with the numerical method. Eq. (8) has been applied to differently sized Mn-Zn ring samples, as illustrated in the example given in Fig. 9, where m = 4.68 and  $f_0 = 3.2 \cdot 10^6$ . It is noted here that only in the largest sample (cross-section of width w = 5.25 mm and height h = 9.72 mm) eddy currents appreciably contribute to W(f) (at least below f = 10 MHz). By subtracting the calculated  $W_{\text{eddy}}^{(\text{cl})}(f)$  from the measured loss, we obtain the eddy current free  $W_{\rm sd}(f)$  behavior (thick solid curves in Fig. 9). The large and the small N30-type ring samples have not the very same structure, resulting into an about 30% different quasi-static loss. But at high frequencies all eddy current free curves merge into a single curve, as expected for a rotations dominated magnetization process. This finding permits us, with little loss of accuracy, to dispense from the complications of the numerical procedure. One can either adjust the value of the constants m and  $f_0$  for best fitting of the eddy current free curve after subtraction of  $W_{\mathrm{eddy}}^{(\mathrm{cl})}(f)$  from the measured W(f) or exploit the general empirical finding that the ratio of the conventional to the actual classical eddy current losses  $R(f) = W_{\text{class}}(f) / W_{\text{eddy}}^{(\text{cl})}(f)$  is a relaxation-type function. At low frequencies this ratio is a precisely known quantity  $R_0$  and we can pose  $R(f) = 1 + \frac{R_0 - 1}{1 + (f/f_1)^2}$ , where the parameter  $f_1$  is again obtained by best fitting of the  $W_{sd}(f)$  curve. In this way we are finally left to justify the  $W_{\rm sd}(f)$  behaviour, which, in many practical samples (as in the example given in Fig. 8), is coincident with the W(f) behavior. The physical mechanism lying behind the energy dissipation is the damping of the precessional motion of the spin moments, taking place both inside the moving domain walls and inside the domains. The energy loss in the sample of Fig. 8 all originates from spin damping and is decomposed into dw and rotational contributions. The former can be lumped in the coercivity and the additional dynamic dw effects and we can write  $W_{dw}(f) = W_h + W_{dw,dyn}(f)$ , where  $W_h$  is the hysteresis (quasi-static) loss and  $W_{dw,dyn}(f)$  can be expressed in a way analogous to the standard derivation of the excess loss in metallic alloys [10, 22], the starting point in both cases being an identical equation for the damped motion of the dw [23]. The spin damping coefficient  $\beta_{sd}$  appearing in this equation is related to the Landau-Lifshitz damping constant  $\alpha_{LL}$  by the expression  $\beta_{\rm sd} = (2J_{\rm s}/\mu_0\gamma\delta)\cdot\alpha_{\rm LL}$ , where  $J_{\rm s}$  is the saturation polarization,  $\mu_0$  is the magnetic constant,  $\gamma$  is the electron gyromagnetic ratio, and  $\delta$  is the dw thickness. The viscous response to the applied AC field of the spin moments inside the domains is described by the linear Landau-Lifshitz-Gilbert equation, by which we can obtain analytical formulations for  $\mu'_{rot}$  and  $\mu''_{rot}$ . The pretty low values of the magnetocrystalline anisotropy of the soft ferrites makes the intergrain demagnetizing fields to interfere with the magnetocrystalline anisotropy fields,

been estimated [10, 11] and found to be always negligible with respect to  $W_{\mathrm{eddy}}^{(\mathrm{cl})}$ , which then accounts for the

239

240

241

242

243

244

245

246

247

248

249

250

251

252

253

254

255

256257

258

259

260

261

262

263

264

265

266

267268

269

270

resulting in a distribution of the effective internal anisotropy fields  $H_{k,eff}$ , that is a continuous spectrum of resonance frequencies. The theoretical  $\mu$ 'rot and  $\mu$ ''rot behaviours are obtained assuming that  $H_{k,eff}$  is distributed according to a lognormal function  $g(H_{k,eff}) = \frac{1}{\sqrt{2\pi}\sigma H_{k,eff}} \cdot \exp[-\frac{(\ln(H_{k,eff}) - h}{2\sigma^2}]$ , where  $h = \langle \ln(H_{k,eff}) \rangle$  and  $\sigma$ ,

the standard deviation of  $ln(H_{k,eff})$ , are adjusted for best fitting of the experimental rotational permeabilities, once further integration is made over the isotropic distribution of the easy axes in the sample plane. An example of predictive capability provided by this approach is shown in Fig. 7, regarding the Mn-Zn ferrite type N87, for which where  $\alpha_{LL} = 0.04$ , h = 5.3,  $\sigma = 1.2$  have been used. The rotational loss can then be immediately predicted through Eq. (6), resulting in the fitting lines shown in Fig. 10 for three different  $J_p$  values.

### 4. Conclusions.

We have presented and discussed the broadband magnetic behaviour of Mn-Zn and Ni-Zn sintered ferrites, clarifying the respective roles of domain wall displacements and rotational processes in providing the material response from DC to 1 GHz. With the help of permeability disaccommodation measurements, we have been able to quantitatively identify and separate the real and complex permeability components  $\mu'_{dw}$ ,  $\mu'_{rot}$ ,  $\mu''_{dw}$ , and  $\mu''_{rot}$  and, a fortiori, dw  $W_{dw}$  and rotational  $W_{rot}$  energy losses across the whole broad range of frequencies. Evidence is offered for the relaxation character of the dw dynamics, which is completely thwarted by the dissipating mechanisms on entering the MHz range and fully overcome by the rotations. It has been shown that eddy currents can contribute to the magnetic losses in Mn-Zn ferrites, provided the frequency is sufficiently high and the samples are large, as quantitatively predicted by a specific multiscale model relying on the measurement of the electrical resistivity of the material as a function of frequency. It is concluded that, for any defined peak polarization value, an eddy current free  $W_{sd}(f) = W_{sd,dw}(f) + W_{sd,rot}(f)$  curve, independent of sample size, can be recovered for any material, where spin damping is the associated dissipation mechanism. The rotational permeability  $\mu'_{rot}(f)$  and  $\mu''_{rot}(f)$  curves are predicted as solutions of the Landau-Lifshitz-Gilbert equation, under assumed lognormal distribution of the internal effective anisotropy fields, and the associated  $W_{sd,rot}(f)$  behaviour is correspondingly obtained, resulting in good agreement with the experimental results.

 305306

321

322

323

324

325

326

327

328

329

331

332

333

334

335

336

337

338

339

340

341

342

343

344

345

346

347

348

349

#### References

- 307 [1] E.C. Snelling, Soft Ferrites: Properties and Applications, Butterworths, 1988.
- 308 [2] V.T. Zaspalis, M. Kolenbrander, R. Guenther, and P. van der Valk, Loss mechanisms in modern MnZn ferrites for power applications, *Proc.* 9<sup>th</sup> Int. Conf. Ferrites-9, R.F. Sohoo, Ed., San Francisco, 2004, 579-584.
- 311 [3] H. Saotome and Y. Sakaki, Iron loss analysis of Mn-Zn ferrite cores, *IEEE Trans. Magn.*, **33** (1997) 728–312 734.
- J. Hanuszkiewicz, D. Holz, E. Eleftheriou, and V. Zaspalis, Materials processing issues influencing the frequency stability of the initial magnetic permeability of MnZn ferrites, *J. Appl. Phys.* **103** (2008) 103907.
- V. Loyau, G.-Y. Wang, M. Lo Bue, and F. Mazaleyrat, An analysis of Mn-Zn ferrite microstructure by impedance spectroscopy, scanning transmission electron microscopy and energy dispersion spectrometry characterizations, *J. Appl. Phys.* **111** (2012) 053928.
- M. LoBue, V. Loyau, and F. Mazaleyrat, Analysis of volume distribution of power loss in ferrite cores, *J. Appl. Phys.* 109 (2011) 07D308.
   E. Cardelli, I. Fiorucci, and E. Della Torre, Estimation of MnZn ferrite core losses in magnetic
  - [7] E. Cardelli, I. Fiorucci, and E. Della Torre, Estimation of MnZn ferrite core losses in magnetic components at high frequency, *IEEE Trans. Magn.* **37** (2001) 23666.
  - [8] E. Otsuki, S. Yamada, T. Otsuka, K. Shoji, and T. Sato, Microstructure and physical properties of Mn-Zn ferrites for high-frequency power supplies, *J. Appl. Phys.* **69** (1991) 5942-5944.
  - [9] M. Drofenik, A. Znidarsic, and I. Zajc, Highly resistive grain boundaries in doped MnZn ferrites for high frequency power supplies, *J. Appl. Phys.*, **82** (1997), 333-340.
  - [10] F. Fiorillo, C. Beatrice, O. Bottauscio, A. Manzin, and M. Chiampi, Approach to magnetic losses and their frequency dependence in Mn-Zn ferrites, *Appl. Phys. Lett.*, **89** (2006) 122513.
  - [11] F. Fiorillo, C. Beatrice, O. Bottauscio, E. Carmi, Eddy current losses in Mn-Zn ferrites, *IEEE Trans. Magn.* **50** (2014) 6300109.
- 330 [12] J. Smit and H.P.J. Wijn, *Ferrites*, Eindhoven: Philips Technical Library, 1959, p. 236.
  - [13] H. Pascard, Basic concepts for high permeability in soft ferrites, J. Phys. IV (France) 8 (1988) 377-384.
  - [14] G. Bertotti, F. Fiorillo, and M. Pasquale, Reversible and irreversibile magnetization in soft iron-based polycrystalline materials, *J. Appl. Phys.*, **69** (1991), 5930-5932.
  - [15] M.T. Johnson and E.G. Visser, A coherent model for the complex permeability in polycrystalline ferrites, *IEEE Trans. Magn.* **26** (1990) 1987-1989.
  - [16] P. J. van der Zaag, P. J. van der Valk, and M. Th. Rekveldt, A domain size effect in the magnetic hysteresis of NiZn-ferrites, *Appl. Phys. Lett.* **69** (1996) 2927-2929.
  - [17] T. Nakamura, T. Tsutaoka, and K. Hatakeyama, Frequency dispersion of permeability in ferrite composite materials, *J. Magn. Magn. Mater.* **138** (1994) 319-328.
  - [18] T. Tsutaoka, M. Ueshima, T. Tokunaga, T. Nakamura, and K. Hatakeyama, Frequency dispersion and temperature variation of complex permeability of Ni-Zn ferrite composite materials, *J. Appl. Phys.* **78** (1995), 3983-3991.
  - [19] C. Beatrice, O. Bottauscio, and F. Fiorillo, Eddy current and spin damping losses in Mn-Zn ferrites, *J. Jpn. Soc. Powder Metallurgy* **61** (2014), S208-S210.
  - [20] A. Magni, F. Fiorillo, E. Ferrara, A. Caprile, O. Bottauscio, and C. Beatrice, Domain wall processes, rotations, and high-frequency losses in thin laminations, *IEEE Trans. Magn.* **48** (2012) 3796-3799.
  - [21] S. Chikazumi, *Physics of Magnetism*, Wiley, 1964, p. 303.
  - [22] F. Fiorillo, M. Coïsson, C. Beatrice, and M. Pasquale, Permeability and losses in ferrites from dc to the microwave regime, *J. Appl. Phys.* **105** (2009), 07A517.
- 350 [23] J.F. Dillon and H.E. Earl, Jr., Domain wall motion and ferromagnetic resonance in a manganese ferrite, *J. Appl. Phys.* **30** (1959), 202-213.